Spatio-temporal dynamics of a nanosecond pulsed microwave plasma ignited by time reversal

Mazières Valentin[1,2], Romain Pascaud[2], Olivier Pascal[1], Richard Clergereaux[1], Luc Stafford[3], Simon Dap[1], Laurent Liard[1]

[1] Laboratoire LAPLACE, Université Paul Sabatier, 118 route de Narbonne, 31062 Toulouse, France
[2] ISAE-SUPAERO, Université de Toulouse, 10 avenue Edouard Belin, 31055 Toulouse France
[3] Département de physique, Université de Montréal, Montréal, Québec H3C 3J7, Canada

E-mail: `valentin.mazieres@laplace.univ-tlse.fr`

Abstract.

In the present paper, the first spatio temporal characterization of a time reversal microwave plasma generated in argon is provided using imaging. This novel source allows to ignite a plasma at a desired location in a reverberant cavity by focusing the electromagnetic energy in time and space. An important feature is the possibility to control the plasma position only by changing the input microwave waveform. The source is operated in a repetitive pulsed mode with very low duty cycle (typically 5×10^{-2} %). Nanosecond pulses have rise time lower than one nanosecond. The generated plasmas have typical sizes in the millimeter range and are observed for dozens of nanoseconds. The plasma behavior is investigated for different pressures and repetition frequencies. A strong dependence is observed between each discharge pulse suggesting the existence of an important memory effect. The latter is probably due to argon metastable atoms and/or residual charges remaining in the post-discharge and allowing the next breakdown to occur at a moderate electric field.

Contents

1. Introduction

Microwaves discharges are intensively studied as they produce high plasma densities both in high and low-pressure conditions. Produced by travelling-waves as in the case of surfatron [1, 2], by radiating microwave power with a slot antenna (SLAN) array [3, 4] or by injecting the wave in closed resonant metallic cavities [5, 6], microwave plasmas are controlled by the balance between [7]:

- the electromagnetic power absorption by the plasma: absorption process takes place through Joule heating of electrons directly controlled by the electric fields.

- the power losses in the plasma volume: losses involve electrons energy transfer to the neutrals and ions by elastic and inelastic collisions as well as gas heating and to the walls by heat conduction and convection.

While inelastic collisions are necessary for plasma ignition, gas and walls heating are limiting processes. Pulsed power can advantageously limit those losses. Indeed, time modulation of power injection has proven to offer different control capabilities of the plasma features [8]. The interruption of the power between repetitive short pulses allows, for example, to constrain the gas heating [9] or to control the chemical processes involved in the plasma volume and on the surfaces [10, 11, 12, 13, 14]. With the electric field intensity, the pulse width w, the repetition rate f_{rep}, the rise and fall times t_r and t_f, as well as the duty cycle D, defined as $D = w.f_{rep}$ are the main parameters that control plasma production and sustainability. A thorough investigation of pulsed microwave plasmas has been conducted on surface-wave-sustained plasmas. For example, Hubner *et al.* and Carbone *et al.* studied pulsed discharges with w down to 1 μs, t_r down to a few tens of ns and $D > 10$ % [15, 9].

A common feature of microwave discharges is the fact that plasma position is controlled and defined by the cavity size and the reactor design (position of the wave launcher, antennas, magnets, etc.). Recently, we have proposed a new kind of microwave plasma source - the so-called "plasma brush" - that allows to produce pulsed discharges with a control of their location independent of the reactor design [16]. In this case the idea is not to create a plasma filling the entire volume of a large plasma vessel, but rather to generate a localized plasma whose position is controlled in real time for local material processing of large objects. This source relies on the control of the waves inside the cavity by modifying the waveform of the input signal. It has been first demonstrated using time reversal (TR) [16] and recently using a more elaborated technique [17]. This requires two steps. In a TR experiment, an emitter first emits a short impulse and the information of the propagation of the waves (impulse response) is recorded using an array of sensors. This is a compulsory learning phase. Then, in order to produce a plasma discharge, this information is time reversed, amplified and re-emitted by the initial sensors. This leads to the reverse scenario: the waves, following the same path but backward, converge toward the initial location of the emission. This results in a spatio-temporal focusing of the electromagnetic energy and possibly a microwave breakdown.

This new plasma source possesses original features: the discharge is produced by focusing microwave energy on a small space ($\lambda_0/2$ in diameter) isolated in the reverberant cavity during a nanosecond pulse width ($w = 8$ ns) in a repetitive mode (typically $f_{rep} = 6$ kHz) corresponding to duty cycles lower than $D = 5{\times}10^{-2}$ %. To the best of our knowledge, microwave plasma sources with such low rise time (in the order of the nanosecond) and such low duty cycle have never been studied. This paper aims to investigate the spatio-temporal behavior of the TR microwave plasmas. Some general features are presented related to the effect of

the pressure (in the range 0.5 - 4 Torr) and of the repetition rate.

2. Plasma source and diagnostic tools

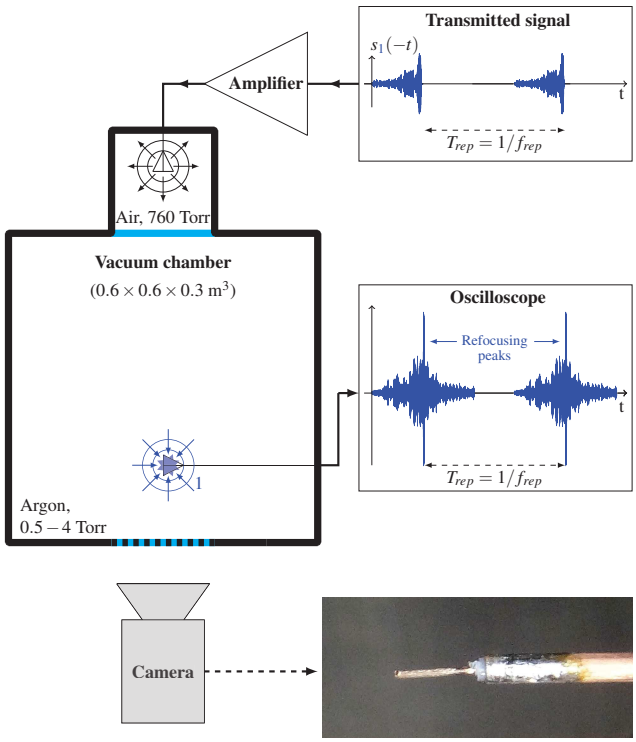

Figure 1. Schematic of the TR plasma source. The signal $s_1(-t)$, *i.e.* the time reversed impulse response between the emitter located in the appendix and the receiver positioned randomly in the reverberant cavity, allows to focus a 8 ns peak near the receiver [16] and to reach plasma breakdown as observed by imaging through a faradized window.

The detailed description of the TR plasma source design and principle have been made in [16]. It is here briefly recalled for the sake of clarity.

Our experimental setup consists of a reverberant metallic cavity with dimensions 0.6 m × 0.6 m × 0.3 m, corresponding to $5\lambda_0 \times 5\lambda_0 \times 2.5\lambda_0$ at the microwave carrier frequency $f_0 = 2.55$ GHz. As schematized in Figure 1, two coaxial probes acting as monopoles are used. The first one, located in an appendix at atmospheric pressure and connected to the main cavity through a glass window, is used as the emitter. The second one, located in the main cavity, is used as the receiver. The main cavity is pumped down using a primary pump. In these experiments, argon is used. It is injected at a constant flow rate controlled by a needle valve to a working pressure p ranging from 0.5 to 4 Torr.

TR signal is defined following two steps [16]. First, a pulse of width $w = 8$ ns, modulated at a carrier frequency $f_0 = 2.55$ GHz, is applied on the receiver and the impulse response $s_1(t)$ between both monopoles is recorded. This signal is then time reversed $s_1(-t)$ and transmitted through the cavity by the emitter in the second step. This complex transmitted signal, shwon in Figure 1, generates a spatio-temporal focusing peak of $w = 8$ ns of dimension $\lambda_0/2 = 6$ cm on the receiver (Figure 1). Note that, as demonstrated in [16], the location of the focusing inside the vacuum chamber is controlled by the waveform of the transmitted signal. As shown in Figure 1, the electrical signal received by the receiver is measured using an oscilloscope (Keysight MSO9254A). The power of the refocusing peak, defined as the square of the measured voltage over the input impedance of the oscilloscope (50 Ω), is proportional to the electric field near the receiving monopole at the focusing instant. However, due to the presence of a very diffusing environment between the monopoles (the reverberant cavity) and the use of broadband signals (bandwidth of 250 MHz), the relationship between this measured power and the value of the electric field is unknown and can not be easily estimated. Therefore, only relative measurements can be performed and power is given in arbitrary units.

In order to reach plasma breakdown condition, the signal $s_1(-t)$ is amplified using a traveling wave tube (TWT) pulsed power amplifier (TMD PTC7353) before being transmitted to the cavity [16]. Note that, in the measurements reported in this paper, the input signal $s_1(-t)$ is injected with the same maximal power level of about 1 kW, unless otherwise specified. The power of the refocusing peak, which is proportional to the maximal input power, that is found in this condition is defined as $P = 7$ arb. units.

In addition to the electrical measurements, optical diagnostics are also performed. It consists in imaging using a camera (PI-MAX-512) that enables to measure the spatio-temporal evolution of the light intensity emitted by the plasma during the signal period. All of the camera measurements presented in this paper are performed without any filter. The camera is triggered by the control device of the amplifier, to synchronize the 4 ns gate time to the TR signal, with the adjusted delay. Each picture results from the accumulation of 20 different gates with a repetition rate of 10 Hz.

3. Experimental results

3.1. Electrical measurements

Two typical signals measured on the receiver during TR experiments are plotted on Figure 2. The

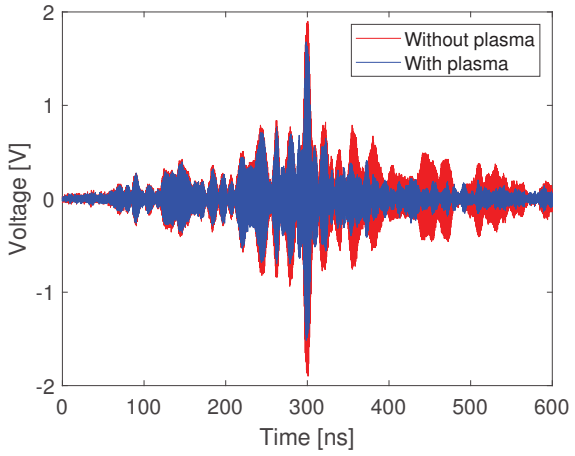

Figure 2. Electrical signals measured on the receiver during a TR experiment. The red curve corresponds to the TR signal at atmospheric pressure, *i.e.* in a condition below the plasma breakdown and the blue one in an Ar plasma ($p = 1.5$ Torr and $f_{rep} = 6$ kHz).

red curve corresponding to a condition below the breakdown condition (*i.e.*, at atmospheric pressure, where there is no evidence of plasma production at naked eyes) shows the TR refocusing peak at $t = 300$ ns with a duration of about 8 ns, similar, as expected, to the one of the initial pulse width w [18]. This peak is surrounded by side lobes before and after the refocusing peak as classically reported in TR experiments in reverberant cavities [19, 20, 18]. The "temporal peak-to-noise" ratio used to characterize the quality of a TR process [18] is estimated for our experimental setup between 4 and 5 [16]. This ratio is linked to the quantity of uncorrelated information and depends on the bandwidth of the initial pulse (here of about 250 MHz) and of the cavity characteristics (volume compared to the wavelength and losses).

For comparison, the signal measured with plasma ($p = 1.5$ Torr, $f_{rep} = 6$ kHz) is reported in blue on Figure 2. The signal remains very similar until the refocusing peak at $t = 300$ ns. A relative comparison of levels before or after the TR refocusing peak and plasma ignition is meaningful. At first sight, one could hope to obtain data such as the absorbed energy by comparing those signals. However, the presence of the plasma near the monopole changes its sensitivity, *i.e.*, the relation between the electric field applied to the monopole and the resulting voltage actually measured with the oscilloscope. Furthermore, depending on the plasma density, the waves may be more or less reflected by the plasma, leading to a lower level of the measured signal. Hence, the analysis cannot go further and absolute data cannot be obtained from that measurements limiting to a global observation of signal lowering and phase-shifting when the plasma is ignited.

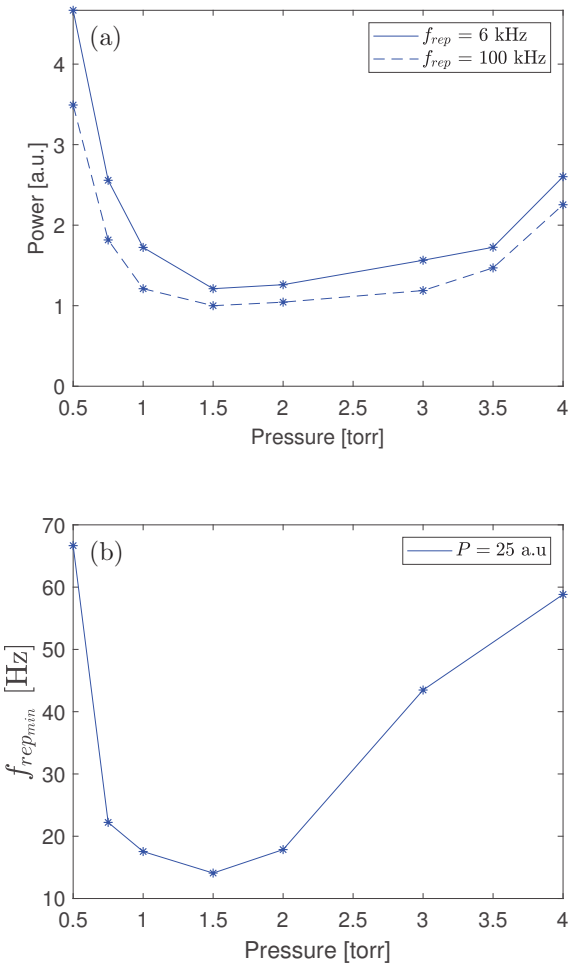

Figure 3. (a) Minimum microwave power and (b) minimum repetition frequency of the TR peak needed to maintain a plasma as a function of the pressure. In both cases, these values were determined from the disappearance of the discharge at naked eyes.

Although for pulsed plasma sources the classical maintain curves, *i.e.*, the minimal sustaining power versus pressure is not so relevant, as a single plasma discharge depends on the previous one, it enables to define at least the operating domain. Here, the following procedure is used to determine the maintain power. At a fixed gas pressure and repetition rate, the discharge is ignited by TR using a high power refocusing peak. Then, the power is smoothly decreased to the minimum value allowing to maintain the discharge. Below this threshold power, the plasma vanishes. These maintain curves are determined for two different repetition rates as plotted on Figure 3(a). The curves show a minimum maintain power near the condition $p = 1.5$ Torr. Considering the classical theory of power deposition in high frequency plasmas, as described *e.g.* in [21], the power density absorbed

by the plasma is given by:

$$P_{abs} = \theta_e n_e \qquad \text{where} \qquad \theta_e = \frac{e^2}{m_e} E_0^2 \frac{\nu_m}{\nu_m^2 + \omega_0^2} \quad (1)$$

with θ_e the power absorbed by an electron, n_e, m_e and e the electron density, mass, and charge, respectively, ν_m the electron neutral momentum collision frequency, ω_0 the wave pulsation, and E_0 the electric field needed to maintain the plasma. The minimum of maintain power around $p = 1.5$ Torr means that the energy transfer is maximal around this pressure, *i.e.*, that the ratio $\frac{\nu_m}{\nu_m^2+\omega^2}$ is maximum for $\nu_m = \omega_0$. Considering that the bandwidth of the microwave signal (250 MHz) is small compared to the carrier frequency f_0, ω_0 can be approximated to be $2\pi f_0 \approx 16 \times 10^9$ rad/s. We can deduce a ν_m of about 16 GHz at 1.5 Torr in our experiments, in good agreement with data found in the literature in these conditions [22].

Regarding the repetition rates, one can expect that with duty cycles $D < 5{\times}10^{-2}$ %, the influence of the previous pulse would disappear and that the maintain power is independent of the repetion rate. Nevertheless, Figure 3(a) shows that as the repetition frequency increases, the power needed to maintain the discharge decreases, as reported in [23, 24]. These measurements clearly show some evidence of the influence of the previous pulse on the next one, as classically attributed to "memory effects".

To fully describe this phenomenon, the lowest repetition rate allowing to maintain the discharge is determined. A similar procedure is used to determine this lowest repetition frequency. Here, the discharge is ignited by TR using a high power refocusing peak with a high repetition rate ($P = 25$ a.u. and $f_{rep} = 6$ kHz). For each gas pressure, the repetition rate is smoothly decreased to the minimum threshold value maintaining the discharge. Below this threshold, the plasma vanishes. The lowest repetition rate allowing to maintain the discharge is plotted in Figure 3(b): it shows that the plasma is maintained for repetition rate as low as 12 Hz for the condition of maximal energy transfer found around $p = 1.5$ Torr. It means that the effect of the previous pulse is still present after a time off of approximately 100 ms.

To further investigate these different mechanisms, the dynamics of the discharge is analyzed by imaging.

3.2. Imaging measurements

The spatio-temporal evolution of a typical TR plasma discharge has been monitored using imaging. In agreement with the previous sections, experimental conditions were chosen as $p = 1.5$ Torr and $f_{rep} = 6$ kHz. Figure 4 reports different snapshots recorded along the pulse injection. It shows that the discharge is ignited near the metallic tip of the monopole.

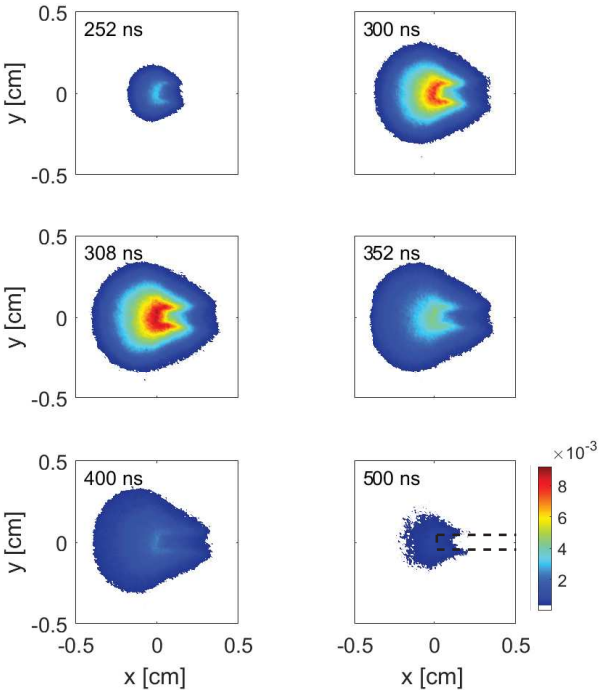

Figure 4. Images of plasma light intensity collected by imaging at $p = 1.5$ Torr and $f_{rep} = 6$ kHz for different times around the TR injection time ($t = 300$ ns). The light intensity is represented as a color map. White parts correspond to the region below a threshold level corresponding to the noise level of the camera measurements and equal to $0.3.10^{-3}$ a.u.. The monopole outline is represented with dashed lines on the image at 500 ns.

It spreads over centimetric distances around the monopole with a quasi-spherical shape and does not move over time. The light intensity profiles along the x and y axes are reported for different instants on Figure 5. In contrast with the light intensity that presents a symmetrical shape along the vertical cut (for x = 0 cm), along a horizontal cut (for y = 0 cm) one can observe a dissymmetry attributed to the presence of the monopole, located from x = 0 cm to the positive x direction, with a diameter of about 0.1 cm on the y axis, symmetrically around x axis. In addition, one can note that the average plasma radius, of about $R_{plasma} = 5$ mm, is smaller than half of the microwave wavelength ($\lambda_0/2$ around 6 cm), which is the dimension of the spatial focusing by TR [18].

Temporal evolutions of the light intensity as well as of the apparent plasma surface are observed around the TR peak. The light intensity integrated across the entire image plotted together with the absolute value of the voltage on Figure 6(a) shows that the light intensity sharply increases when the TR signal is injected up to a maximum at around $t = 308$ ns, *i.e.*, at the end of the TR signal.

After the main TR peak, the light intensity decreases following an exponential decay (scarcely

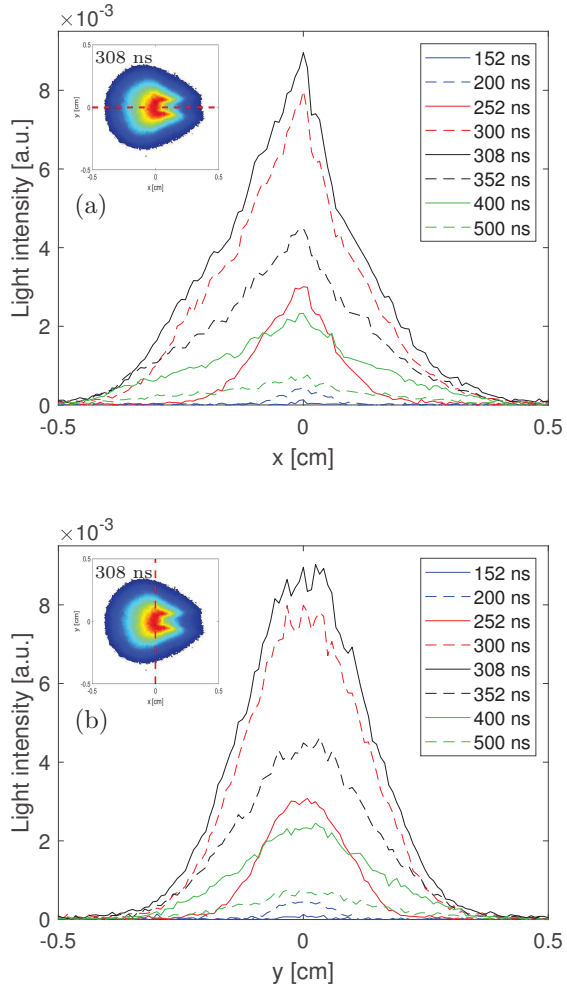

Figure 5. (a) Horizontal cut, meaning along the x axis for y = 0 cm, and (b) vertical cut, meaning along the y axis for x = 0 cm, for different times including the times presented in Figure 4.

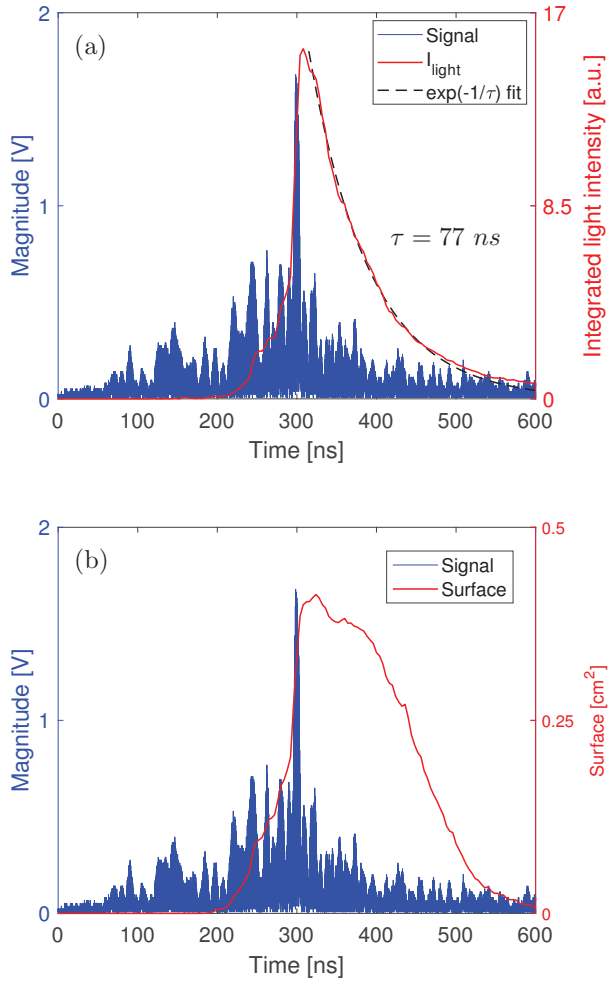

Figure 6. Temporal evolution of (a) the integrated light intensity and of (b) the plasma volume along with the absolute value of the voltage. The volume is defined as the sum of the pixels with light intensity higher than the threshold taken just above the noise level and equal to $0.3.10^{-3}$ a.u. (see Figure 4).

heckled by the effect of the signal side lobes), as shown by the exponential fit reported as a dotted line in Figure 6(a) and called in the following the "early post-discharge". In the condition $p = 1.5$ Torr, $f_{rep} = 6$ kHz, this decay time is estimated around 77 ns. Finally, an attentive observation highlights that the plasma is ignited before the TR signal injection (*e.g.* at $t = 252$ ns *i.e.* 50 ns before), in a so-called "late post-discharge". Indeed, between 220 and 300 ns, light emission is observed and clearly correlated with intense side lobes. The phenomena occuring during these two periods are discussed later in Section 4.

Similar behaviors are observed on the plasma surface as plotted in Figure 6(b): the spatial spreading of the plasma is strongly correlated to the signal measured on the monopole and mainly due to the TR refocused peak. Nevertheless, the surface does not decrease at the end of the TR peak (308 ns) but few tens of ns after with some minor "rebounds" due to signal side lobes.

3.3. Influence of the pressure

Figure 7 shows images of the plasma light intensity at the end of the TR signal ($t = 308$ ns) for a repetition rate fixed at $f_{rep} = 6$ kHz and different gaz pressure.

The pressure has a clear effect on the discharge: when the pressure increases, the plasma becomes more and more compressed near the tip of the monopole. This behavior is typical of diffusion controlled plasmas. As the pressure increases, the collision frequency between charged particles and neutrals increases limiting the diffusion process. It is thus reasonable to assume that a similar process occurs during such transient TR plasmas. As it is localized in front of the monopole tip where the electric field is the higher, the light intensity emitted by the plasma also increases.

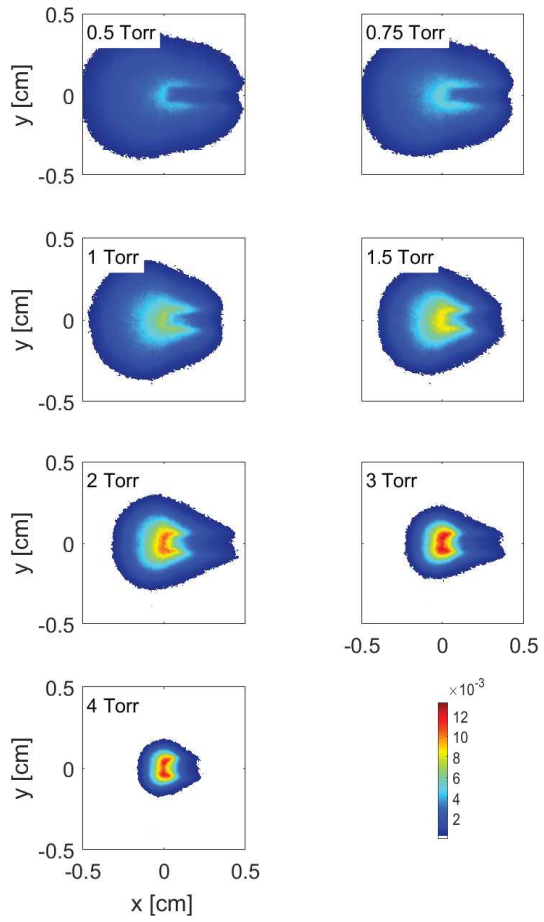

Figure 7. Images of plasma light intensity collected by imaging after the TR peak instant ($t = 308$ ns) for different pressures.

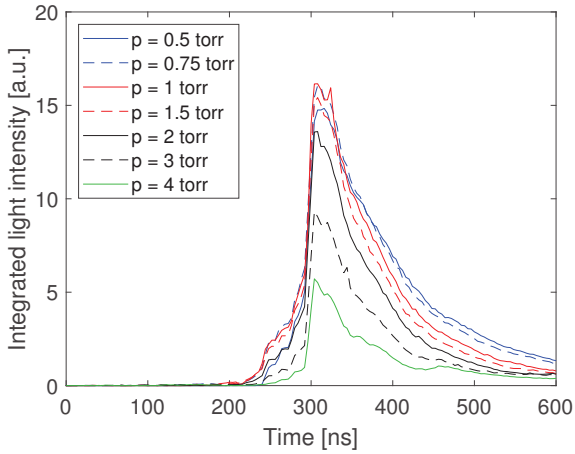

Figure 8. Temporal evolution of the integrated light intensity.

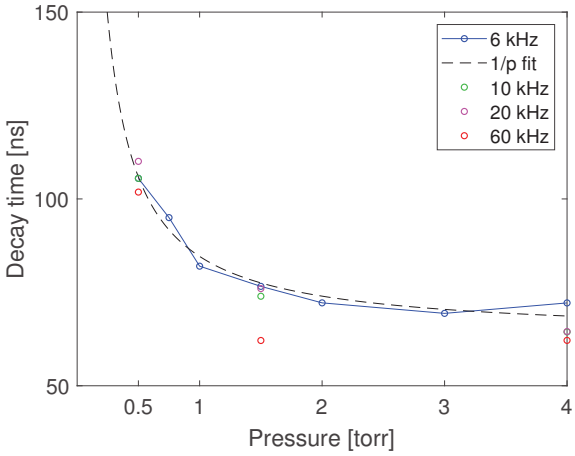

Figure 9. Evolution of the decay time with the pressure, obtained by fitting the data of Figure 8 after the main peak, for different repetition rates.

The temporal evolutions of the integrated light intensity as plotted in Figure 8 show a key role of the working pressure. First, it shows that together with a plasma spatial limitation with the pressure, the maximum of plasma light intensity decreases with the working pressure. The early post-discharge is always characterized by an exponential decay with a decay time, as reported in Figure 9, of few tens of ns. In addition, this shows that this decay time decreases with the pressure from 100 ns at 0.5 Torr down to 65 ns at 4 Torr, following a p^{-1} evolution. Finally, during the late post-discharge, light emission previously correlated with the signal side lobes appears in every condition.

3.4. Influence of the repetition rate

The effect of the repetition rate on the discharge appears to be quite strong as illustrated in Figure 10 for two different repetition frequencies and three different pressures. The dotted lines correspond to the previous case with a repetition frequency of 6 kHz whereas the plain lines correspond to a repetition frequency of 60 kHz. For a given pressure, the integrated light emission increases when increasing the frequency. Moreover, it is more pronounced for higher pressure. In addition, the decay time of the light intensity after the main peak remains almost identical in the 6 - 60 kHz range as summarized in Figure 9. The latter thus seems to be mainly related to the pressure. Finally, the early light emission before the TR peak is also tremendously affected by the increase of the frequency. At 60 kHz, its level can reach up to 40 % of the maximum light emission in good agreement with a memory effect between two TR refocusing peaks.

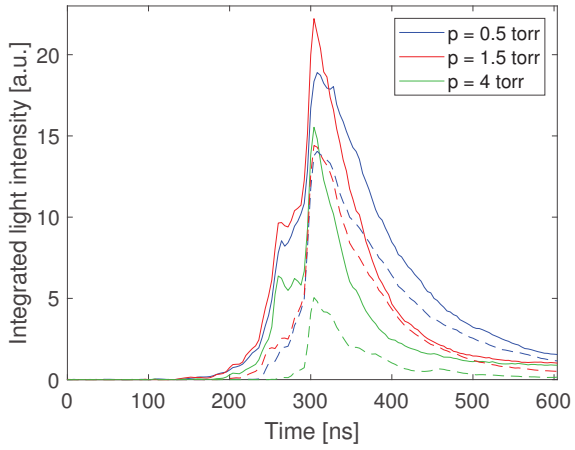

Figure 10. Evolution of the integrated temporal intensity for two different repetition rates, $f_{rep} = 6$ kHz in dotted line and $f_{rep} = 60$ kHz in plain line, and for three pressures $p = 0.5$ Torr (blue), $p = 1.5$ Torr (red) and $p = 4$ Torr (green).

4. Discussion

To describe and analyse TR plasma production, the pulsed discharge will be studied starting from the main TR refocusing peak ($t = 300$ ns) until the next one.

4.1. Refocusing peak

As it was already noticed, the duration of the refocusing peak is quite unusual for microwave plasma sources. Indeed, thanks to TR a high microwave power level is injected around the monopole during $w = 8$ ns with a rise time lower than $t_r = 1$ ns. With the TR technique, the electromagnetic energy injected in the cavity is focused in time and space. This main peak (at 300 ns on the plot), spatially centered on the monopole, triggers an important light emission due to the formation of a plasma discharge. Over the range of experimental conditions investigated, the electron density remains unknown. The only available experimental information is the difference observed in the voltage collected by the monopole after the main peak with and without plasma. This suggests that the electron density changes either the sensitivity of the monopole, *i.e.*, the relationship between the electromagnetic waves at the monopole and the voltage collected, or the propagation of electromagnetic waves at the vicinity of the monopole, or both.

4.2. Early post-discharge

When the main peak has ended, the emission intensity decreases exponentially, only slightly disturbed by the side lobes of the microwave signal. On Figure 9, this decay time is inversely proportional to the pressure. Assuming that light emission predominantly comes from the spontaneous decay of Ar $2p_i$ states and that these levels are mostly excited by electron-impact excitation of ground-state Ar atoms, the total emission intensity can be written as:

$$I_{Total} = \sum_i \frac{hc}{\lambda_i} f(\lambda_i) k_i(T_e) n_e n_{Ar} \tag{2}$$

where h is the Planck constant, c is the speed of light, λ_i is the wavelength of the Ar $2p_i - 1s_j$ transitions, $f(\lambda_i)$ is the optical response of the detection system at wavelength λ_i, $k_i(T_e)$ is the reaction rate for electron-impact excitation of the Ar $2p_i$ state from ground state Ar atoms (a function of the electron temperature, T_e), n_e is the electron density, and n_{Ar} is the number density of ground state Ar atoms. Based on Equation 2, the decay of the total emission intensity in the early post-discharge for a given pressure could be related to a decrease of either the electron density or electron temperature. We now look closer at these different possible causes.

In diffusion-controlled plasmas, charged particles losses are ruled by either free or ambipolar diffusion depending on the absolute number of the electron density (free diffusion in weakly ionized discharges and ambipolar diffusion in more strongly ionized plasmas). In such conditions, the electron density decay time is linked to the characteristic diffusion times that can be estimated using the following equation:

$$\tau_{diff} = \frac{\Lambda^2}{D_{diff}} \tag{3}$$

where Λ is the diffusion length and D_{diff} is the free or ambipolar diffusion coefficient. In spherical geometry, the diffusion length writes $\Lambda = L/\pi$, where L is the characteristic size of the plasma vessel. In our case, there is no correlation between the typical size of the plasma and the vessel dimension. Consequently, L is set equal to a typical plasma radius, *i.e.* $L = 5$ mm. Considering an electron temperature T_e of about 2 eV in a 1.5 Torr Ar plasma, the characteristic time is tens of nanoseconds for the free diffusion regime and tens of microseconds in the ambipolar regime. Note that in this last case, electron-ion recombination can shorten the electron density decay time as shown by Hubner *et al.* [15]. In any case, as the working pressure increases, the characteristic diffusion coefficient decreases such that the electron density decay time (Equation 3) increases, which is inconsistent with the set of data presented in Figure 9.

Electron energy relaxation following the extinction of the microwave signal can also induced a decrease of the total emission intensity in the early post-discharge. Neglecting power deposition and heat

transport phenomena, the energy balance equation for electrons can be written as [22] :

$$\frac{dT_e}{dt} = -n_n \left(\sum_j k_j(T_e)\epsilon_j \right) \quad (4)$$

where n_n is the neutral density, $k_j(T_e)$ is the reaction rate for electron-atom collisions (elastic and inelastic collisions), and ϵ_j is electron energy loss per electron-atom collision. Here, the summation takes into account electron momentum transfer collisions as well as electron-impact excitation and ionization processes [22]. From the corresponding set of reaction rates, this non-linear differential equation can be numerically resolved using the number density of ground state Ar atoms and the initial value of the electron temperature T_{e_0} as the only adjustable parameters. It is worth highlighting that for argon plasmas with electron temperatures of a few eV, electron energy relaxation is dominated by excitation and ionization processes. Considering an initial electron temperature of 2 eV in a 1.5 Torr Ar plasma, $T_e(t)$ and thus $I_{Total}(t)$ can thus be calculated using Equations 4 and 2, respectively. In such conditions, using the set of cross sections described in [25] the characteristic decay time of the total emission intensity is around 100 ns, which is comparable to the experimental data. Moreover, Equation 4 reveals that the electron energy relaxation time is inversely proportional to the number density of ground state Ar atoms, which is in very good agreement with the set of data presented in Figure 9. Therefore, over the range of experimental conditions investigated, the observed exponential decay time of the total emission intensity in the early post-discharge is mostly linked to the electron energy relaxation as the electron density decay time is much longer.

4.3. Late post-discharge

Between two pulses, once T_e has relaxed as discussed in the previous section, one can assume a classical post-discharge evolution, with densities of charged species and metastable states evolving together. Experimental measurements reported in the previous sections clearly show the existence of a memory effect resulting from previous discharges and influencing the development of the following ones. This effect often occurs in discharges working in repetitive mode. It is related to the persistence of species such as electrons, ions, metastable states or radicals, from one discharge to the following one. Various mechanisms can be involved in the memory effects, their occurrence being strongly determined by the operating conditions such as the gas composition, pressure, discharge type... It can promote the ignition of the next discharge [26, 9, 27, 28] *e.g.* because of the presence of seed electrons, or on the contrary perturb the next discharge *e.g.* if the remaining ion density is sufficient to disturb the electric field [29, 30].

Assuming an electron temperature of 300 K, a new estimation of the characteristic diffusion times of charged particles can be provided. For this very low electron temperature, an approximated collision rate of 2×10^{-15} m^3s^{-1} is used [22]. The resulting characteristic diffusion times for a pressure of 1 Torr are 20 ns and 500 μs for the free and ambipolar diffusion respectively. Thus, if the plasma is sufficiently dense for the ambipolar process to rule the diffusion of free charges, a non-negligible amount of charges can remain in the medium until the next pulse. Electron-ion recombination can also play a role as previously mentioned. The dissociative recombination (DR) process $Ar_2^+ + e \rightarrow Ar^* + Ar$ generally plays a major role at the very beginning of the post-discharge whereas the collisional-radiative (CR) recombination $Ar^+ + e + e \rightarrow Ar^* + e$ dominates at larger time scale when the electron temperatures becomes very low [31]. Their respective coefficients can be found in [32] for (DR) recombination and [33] for (CR) recombination. Depending on the plasma density, simple calculations indicate that electrons can remain in the medium for dozens of ms after the pulse. Nevertheless, it is interesting to note that these processes do not only result in charged particles losses but also in the production of metastable argon atoms. Metastable atoms coming either from the discharge or from recombination processes can play an important role in the memory effect as shown *e.g.* by Carbone *et al.* [9]. Based on [34], the lifetime of the $Ar(^3P_2, 1s_5)$ metastable state is essentially determined by the rate of two- and three-body collisional deexcitation with neutral argon. Indeed, the low electron temperature makes unlikely any process involving energetic electrons such as excitation towards upper levels or mixing of the metastable and resonant 1s argon state [31]. It results in an $Ar(^3P_2, 1s_5)$ lifetime at 1.5 Torr around 10 ms. Thus, for $f_{rep} \geq 100$ Hz, metastables can greatly facilitate the breakdown before the next TR peak through step-wise processes. The presence of residual charges and metastable atoms in the late post-discharge are thus probably responsible for the observed memory effect. It explains the early light emission observed during the first side lobes of the voltage magnitude and the strong dependence of the breakdown behavior with respect to the operating conditions such as the repetition frequency. This behavior can be referred as ionization in moderate electric field.

5. Conclusions

Time reversal plasmas are pulsed discharges produced by refocusing microwave power. This paper brings the first insight on the microwave TR plasma properties. Indeed, TR allows to generate microwave plasmas as short as $w = 8$ ns with repetition rate down to $f_{rep} = 12$ Hz resulting, to the best of our knowledge, in the very lowest duty cycle pulsed discharge with $D < 10^{-2}$ %. It works at low pressure with a condition of maximal energy transfer in argon around 1.5 Torr. The size of the generated plasmas was found with centimetric dimension, *i.e.*, lower than the microwave wavelength. The latter is an important aspect of this source as the plasma and the cavity dimensions are uncorrelated making the mechanisms involved in ignition and afterglow phases unusual.

From the spatio-temporal dynamics of TR plasmas, three different steps are identified. First, when the microwave power is focused around the monopole, plasma breakdown condition is reached as observed by the sharp increase of the light intensity. The power deposition leading to the plasma ignition is followed by a post-discharge. Early, the light intensity was found to decrease exponentially with a characteristic decay time of about tens of nanoseconds inversely proportional to the pressure and independent on the repetition rate. This behavior was attributed to electron energy dissipation due to collisions with the background gas. In addition, a late post-discharge mechanism plays also a role in the discharge dynamics. It is probably related to the presence of energetic species and/or residual charges, which submitted to moderate electric field, *i.e.*, of the side lobes - inherent to TR process and observed 100 ns before the main TR peak - allow the ionization of the gaz, especially in low pressure and high repetition frequency conditions. This strong dependence regarding experimental conditions confirms the importance of a memory effect. Future work will be devoted to a deeper understanding of its fundamental parameters.

6. Acknowledgments

The authors would like to acknowledge the DGA/AID for their funding support and the CEA-Gramat for the material support.

References

[1] Moisan M, Zakrzewski Z and Pantel R 1979 *J. Phys. D: Appl. Phys.* **12** 219–237 ISSN 0022-3727 publisher: IOP Publishing

[2] Moisan M and Zakrzewski Z 1991 *J. Phys. D: Appl. Phys.* **24** 1025–1048 ISSN 0022-3727 publisher: IOP Publishing

[3] Conrads H and Schmidt M 2000 *Plasma Sources Sci. Technol.* **9** 441–454 ISSN 0963-0252 publisher: IOP Publishing

[4] Korzec D, Werner F, Winter R and Engemann J 1996 *Plasma Sources Sci. Technol.* **5** 216–234 ISSN 0963-0252 publisher: IOP Publishing

[5] Asmussen J, Mallavarpu R, Hamann J and Park H C 1974 *Proceedings of the IEEE* **62** 109–117 ISSN 1558-2256

[6] Hagelaar G J M, Hassouni K and Gicquel A 2004 *Journal of Applied Physics* **96** 1819–1828 ISSN 0021-8979 publisher: American Institute of Physics

[7] Asmussen J 1989 *Journal of Vacuum Science & Technology A* **7** 883–893 ISSN 0734-2101 publisher: American Vacuum Society

[8] Rousseau A, Tomasini L, Gousset G, Boisse-Laporte C and Leprince P 1994 *J. Phys. D: Appl. Phys.* **27** 2439–2441 ISSN 0022-3727 publisher: IOP Publishing

[9] Carbone E, Sadeghi N, Vos E, Hübner S, Veldhuizen E v, Dijk J v, Nijdam S and Kroesen G 2014 *Plasma Sources Sci. Technol.* **24** 015015 ISSN 0963-0252

[10] Martin P M 2009 *Handbook of deposition technologies for films and coatings: science, applications and technology* (Norwich, N.Y.; Oxford: William Andrew ; Elsevier Science [distributor) ISBN 978-0-8155-2031-3 oCLC: 500570903

[11] Hassouni K, Duten X, Rousseau A and Gicquel A 2001 *Plasma Sources Sci. Technol.* **10** 61–75 ISSN 0963-0252 publisher: IOP Publishing

[12] Heintze M, Magureanu M and Kettlitz M 2002 *Journal of Applied Physics* **92** 7022–7031 ISSN 0021-8979 publisher: American Institute of Physics

[13] Cunge G, Bodart P, Brihoum M, Boulard F, Chevolleau T and Sadeghi N 2012 *Plasma Sources Sci. Technol.* **21** 024006 ISSN 0963-0252 publisher: IOP Publishing

[14] Bousquet A, Granier A, Goullet A and Landesman J P 2006 *Thin Solid Films* **514** 45–51 ISSN 0040-6090

[15] Hübner S, Palomares J M, Carbone E A D and Mullen J J A M v d 2012 *J. Phys. D: Appl. Phys.* **45** 055203 ISSN 0022-3727 publisher: IOP Publishing

[16] Mazières V, Pascaud R, Liard L, Dap S, Clergereaux R and Pascal O 2019 *Appl. Phys. Lett.* **115** 154101 ISSN 0003-6951

[17] Mazières V, Al Ibrahim A, Chauvière C, Bonnet P, Pascaud R, Clergereaux R, Dap S, Liard L and Pascal O 2020 *IEEE Access* 1–1 ISSN 2169-3536

[18] Lerosey G, de Rosny J, Tourin A, Derode A, Montaldo G and Fink M 2004 *Phys. Rev. Lett.* **92** 193904

[19] Draeger C, Aime J C and Fink M 1999 *The Journal of the Acoustical Society of America* **105** 618–625 ISSN 0001-4966 publisher: Acoustical Society of America

[20] Draeger C and Fink M 1999 *The Journal of the Acoustical Society of America* **105** 611–617 ISSN 0001-4966 publisher: Acoustical Society of America

[21] Moisan M and Pelletier J 2012 *Physics of Collisional Plasmas: Introduction to High-Frequency Discharges* (Springer Netherlands) ISBN 978-94-007-4557-5

[22] Lieberman M A and Lichtenberg A J 2005 *Principles of Plasma Discharges and Materials Processing , 2nd Edition* 2nd ed (Hoboken, N.J: Wiley-Interscience) ISBN 978-0-471-72001-0

[23] Dawson E F and Lederman S 1973 *Journal of Applied Physics* **44** 3066–3073 ISSN 0021-8979

[24] Vikharev A L, Ivanov O A and Stepanov A N 1985 *Radiophysics and Quantum Electronics* **28** 26–31 ISSN 0033-8443

[25] Durocher-Jean A, Desjardins E and Stafford L 2019 *Physics of Plasmas* **26** 063516 ISSN 1070-664X publisher: American Institute of Physics

[26] Massines F, Gherardi N, Naudé N and Ségur P 2009 *Eur. Phys. J. Appl. Phys.* **47** 22805 ISSN 1286-0042, 1286-0050 number: 2 Publisher: EDP Sciences

[27] Osawa N and Yoshioka Y 2012 *IEEE Transactions on Plasma Science* **40** 2–8 ISSN 1939-9375 conference Name: IEEE Transactions on Plasma Science
[28] Lin X, Tyl C, Naudé N, Gherardi N, Popov N A and Dap S 2020 *J. Phys. D: Appl. Phys.* **53** 205201 ISSN 0022-3727 publisher: IOP Publishing URL
[29] Kazemi M R, Sugai T, Tokuchi A and Jiang W 2017 *IEEE Transactions on Plasma Science* **45** 2323–2327 ISSN 1939-9375 conference Name: IEEE Transactions on Plasma Science
[30] Zhao Z, Huang D D, Wang Y N, He J X, Li C J, Wang Y F and Li J T 2019 *Plasma Sources Sci. Technol.* **28** 085015 ISSN 0963-0252 publisher: IOP Publishing URL
[31] Carbone E, Dijk J v and Kroesen G 2015 *Plasma Sources Sci. Technol.* **24** 025036 ISSN 0963-0252 publisher: IOP Publishing
[32] Mehr F J and Biondi M A 1968 *Phys. Rev.* **176** 322–326 publisher: American Physical Society
[33] Biberman L M, Vorob'ev V S and Yakubov I T 1987 *Kinetics of Nonequilibrium Low-Temperature Plasmas* (Springer US) ISBN 978-1-4684-1667-1
[34] Stefanović I, Kuschel T, Schröter S and Böke M 2014 *Journal of Applied Physics* **116** 113302 ISSN 0021-8979 publisher: American Institute of Physics